Simplified Theory for Linear Rheology of Monodisperse Linear Polymers

Marie-Claude Heuzey,[1] Paula Wood-Adams,[2] Djamila Sekki[1]

[1]*Center for Applied Research on Polymers (CRASP), Department of Chemical Engineering, École Polytechnique de Montréal, P.O. Box 6079, Stn. Centre-ville, Montreal, QC H3C 3A7, Canada*
[2]*Department of Mechanical and Industrial Engineering, Concordia University, 1455 de Maisonneuve Blvd. West, Suite H-549, Montreal, QC H3G 1M8, Canada*

Received 18 February 2004; accepted 19 April 2004
DOI 10.1002/app.20881
Published online in Wiley InterScience (www.interscience.wiley.com).

ABSTRACT: A new version of the tube theory based on the de Gennes–Doi–Edwards reptation concept (reported in Likhtman and McLeish's work published in 2002) is evaluated, modified to allow for simplified computations, and used to study the relationship between zero-shear viscosity and molecular weight for monodisperse entangled linear homopolymers. The Likhtman–McLeish model combines self-consistent theories for contour length fluctuations and constraint release with reptation theory for monodisperse linear polymers. Because of the nature of the Rubinstein and Colby approach used for the treatment of constraint release, the related term is probabilistic and requires stochastic simulations for the calculation of the relaxation modulus $G(t)$. This makes the Likhtman–McLeish model computationally difficult to use. In this work we solve this problem by generating an approximate closed-form solution for the stochastic term. Then analytical integration of the relaxation modulus function $G(t)$ provides an expression for the zero-shear viscosity (η_0). Results of the computations of the zero-shear viscosity and of the slope of η_0 versus molecular weight are compared with available experimental data for monodisperse entangled linear polystyrene and polyethylene (hydrogenated polybutadiene). The model is a major improvement over previous theoretical models, even if there is still some disagreement between the predictions and experimental data of the slope of η_0 versus molecular weight. The possibility of inferring monomer chemistry–dependent parameters from the zero-shear viscosity remains a difficult task because of the introduction of a constraint-release parameter. Nevertheless, the model is a useful tool for the prediction of linear viscoelasticity data. © 2004 Wiley Periodicals, Inc. J Appl Polym Sci 94: 569–586, 2004

Key words: viscoelastic properties; viscosity; monodisperse polymers; relaxation; shear

INTRODUCTION

Early molecular theories designed to represent the dynamics of entangled polymers have been fairly successful qualitatively, but in general have been lacking quantitative agreement. For example, the reptation theory originally proposed by de Gennes,[1] and later generalized by Doi and Edwards,[2] predicted a scaling of the zero-shear viscosity with the cube of the polymer molecular weight, whereas it was experimentally shown that the power-law index was 3.4 over a considerable range of molecular weights for many polymers. Some experimental investigations have also obtained exponents ranging from 3.3 to 3.7.[3]

Intensive theoretical efforts have been devoted in the last two decades to improve the predictions of the reptation-based tube model. A new modification of the de Gennes–Doi–Edwards reptation concept (Likhtman and McLeish[4]) was recently proposed for monodisperse linear entangled homopolymers with two main improvements to enhance agreement with experimental data. The Likhtman–McLeish model combines self-consistent theories for contour length fluctuations (CLF) and constraint release (CR) with reptation theory. Improvement of the treatment of contour length fluctuations was achieved by using a combined theoretical and stochastic simulation approach, which results in a closed-form single-chain relaxation function $\mu(t)$ without any adjustable parameters or approximations. Constraint release is included by using the scheme proposed by Rubinstein and Colby.[5] This approach allows the calculation of a constraint-release term, $R(t)$, from the single-chain relaxation function. Because of the nature of the Rubinstein and Colby approach, the term $R(t)$ is probabilistic, requiring stochastic simulations for the calculation of the relaxation modulus $G(t)$. Longitudinal Rouse relaxation along the chain is also taken into account in the model. Likhtman and McLeish[4] showed that accurate treatment of both CLF and CR can capture quantitatively experimental observations. However, because of the

Correspondence to: M.-C. Heuzey (marie-claude.heuzey@polymtl.ca).

stochastic term, the model is computationally intensive. The objective of this work is to present an approximate closed-form version of the Likhtman–McLeish model to simplify its use. In addition, analytical integration of the material relaxation function $G(t)$ is performed to obtain an expression for the zero-shear viscosity (η_0). This zero-shear viscosity model is compared with available experimental data for monodisperse entangled linear homopolymers. The possibility of inferring monomer chemistry–dependent parameters from the zero-shear viscosity is discussed.

PHYSICAL PROCESSES IN THE TUBE MODEL

Reptation theory reduces the confinement of a high molecular weight polymer by surrounding chains to a tubular region. Motions perpendicular to the tube are prohibited, whereas those parallel to the tube axis (the primitive path) are allowed. The diffusion of the polymer out of its tube is called reptation and is the main dynamic mode of all tube models for entangled linear polymers. However, as mentioned in the introduction, the original reptation theory was unable to correctly fit experimental linear relaxation moduli G' and G'' and did not properly describe η_0 dependency with molecular weight. This is because several important physical processes were missing from the original theory: (1) contour length fluctuations (CLF), (2) constraint release (CR), and (3) longitudinal stress relaxation along the tube. Contour length fluctuations correspond to a more detailed description of the escape motion of a single chain out of its tube, taking into account fluctuations of the path length by the inclusion of all Rouse modes (bead-and-spring model). Constraint release accounts for the movement of the tube resulting from the movements of the surrounding chains. Finally, longitudinal stress relaxation, which is also derived from the bead-and-spring model, must not be confused with CLF. Although CLFs describe the escape from the tube by path fluctuations, longitudinal relaxation is related to the motion inside the tube and counts for 1/5 of the stress relaxation. A more detailed description of each of these physical processes is given by Likhtman and McLeish.[4]

In the past, incorporation of CLF into the Doi–Edwards (DE) model improved the power-law scaling of the zero-shear viscosity with molecular weight (Doi[6] and Milner and McLeish[7]). The addition of the CR mechanism allowed an improvement in the description of oscillatory flow behavior, especially for polydisperse systems (des Cloiseaux[8]). Finally, consideration of longitudinal relaxation remarkably improved the theoretical predictions of G' and G'' for multiarm star/linear polymer mixtures (Miros et al.[9]).

The mechanisms depicted above are now relatively well established. There is a consensus within the tube theory community about which physical processes should be accounted for in the tube representation of polymer melt behavior. In their work on the theory of linear dynamics of linear entangled polymers, Likhtman and McLeish[4] do not introduce any new physical processes. Instead, they propose a more accurate mathematical representation of the single-chain relaxation function, which describes the relaxation of the chain in its original tube, and then they self-consistently and simultaneously solve this and existing mathematical models describing the accepted physical processes. They show that accurate and enhanced treatment of both CLF and CR can capture most experimental observations.

However, when nonlinear flows or large step strain experiments are encountered, convected constraint release (CCR), introduced by Marucci,[10] becomes the main mechanism of relaxation. A new stochastic microscopic theory[11] based on the tube model and including CCR has shown good agreement with experiments over a wide range of rheological data, for entangled polymer solutions in nonlinear shear and extension. A macroscopic version of that model in the form of a simple differential constitutive equation for linear polymers has recently been presented.[12] Although this model has been developed for nonlinear flows, it can naturally be used in the limit of the linear viscoelastic regime. However, the macroscopic version of the model requires the fitting of a set of G_e^i–τ_e^j parameters, or a discrete spectrum, which are not representative any longer of the material molecular structure. In this work, we present a simplified version of the Likhtman–McLeish theory for linear rheology,[4] which retains a relationship to molecular structure by the use of monomer-dependent parameters.

MATHEMATICAL TREATMENT OF THE PHYSICAL PROCESSES

Reptation and contour length fluctuations

According to the Likhtman–McLeish model, the starting point of the solution of the full problem is the calculation of the single-chain relaxation function $\mu(t)$, which is attributed to the escape of the single chain from its original tube. Simultaneous treatment of CLF and reptation by using a combined theoretical and stochastic simulation approach results in a single-chain relaxation function $\mu(t)$ described at all times by

$$\mu(t) = \frac{8\tilde{G}_f}{\pi^2} \sum_{p=1,odd}^{p^*} \frac{1}{p^2} \exp\left(-\frac{tp^2}{\tau_{df}}\right) + \int_{\varepsilon^*}^{\infty} \frac{0.306}{Z\tau_e^{1/4}\varepsilon^{5/4}} \exp(-\varepsilon t)\, d\varepsilon \quad (1)$$

The first term represents reptation and the second one CLF. The parameter Z is defined as the number of tube segments (i.e., $Z = N/N_e$), where N is the number of monomers with friction coefficient ζ contained in each chain, and N_e is the number of monomers per tube segment (i.e., $N_e = a^2/b^2$), where a is the tube diameter and b the Kuhn segment. The parameter Z is also related to the entanglement molecular weight M_e, as $Z = M/M_e$, where M is the molar mass of the chain. Other parameters of eq. (1) are defined as follows:

—τ_e is the Rouse time of an entanglement length:

$$\tau_e = \frac{N_e^2 \zeta b^2}{3\pi^2 k_B T} \tag{2}$$

where k_B is the Boltzmann constant and T is the temperature.

—$\tilde{G}_f(Z)$ and $\tau_{df}(Z)$ are renormalizations of the dimensionless plateau modulus and the reptation time attributed to CLF:

$$\tilde{G}_f(Z) = 1 - \frac{2C_1}{\sqrt{Z}} + \frac{C_4}{Z} + \frac{C_5}{Z^{3/2}} \tag{3}$$

$$\frac{\tau_{df}(Z)}{\tau_d^{(0)}(Z)} = 1 - \frac{2C_1}{\sqrt{Z}} + \frac{C_2}{Z} + \frac{C_3}{Z^{3/2}} \tag{4}$$

with $C_1 = 1.69$, $C_2 = 4.17$, $C_3 = -1.55$, $C_4 = 2.0$, and $C_5 = -1.24$.

—The reptation or disentanglement time is $\tau_d^{(0)} = 3Z^3\tau_e$.

—Finally, p^* is chosen as $\sqrt{Z/10}$, and

$$\varepsilon^* = \frac{1}{\tau_e Z^4}\left(\frac{4 \times 0.306}{1 - \frac{8\tilde{G}_f}{\pi^2}\sum_{p=1,odd}^{p^*}\frac{1}{p^2}}\right) \tag{5}$$

Constraint release

Constraint release is related to the evolution of the tube, given that the tube is made from surrounding chains, which are moving. To obtain a quantitative result, different tube segments should be assigned different mobilities m_i, given that the mobilities are distributed quite widely if CLF is taken into account. The most detailed self-consistent algorithm, which considers a distribution of tube segment mobilities, and allows one to obtain the material relaxation function $G(t)$ from the single-chain distribution $\mu(t)$, was developed by Rubinstein and Colby.[5] This algorithm consists of several steps. First, the inverse Laplace transform $P(\varepsilon)$ of $\mu(t)$ is determined:

$$\mu(t) = \int_0^\infty P(\varepsilon)\exp(-\varepsilon t)\, d\varepsilon \tag{6}$$

Then, one assumes that the mobilities of the tube segments m_i are distributed according to $P(\varepsilon)$, where $\varepsilon/k < m < (\varepsilon + d\varepsilon)/k$ and where k is the elastic constant of the sections of the chains of one entanglement length long. $P(\varepsilon)$ should satisfy the normalization condition $\int P(\varepsilon)\, d\varepsilon = \mu(0) = 1$. The second step consists in finding the spectrum of relaxation rates $dM(\varepsilon)/d\varepsilon$, where $M(\varepsilon)$ is defined as the number of relaxation modes slower than ε. More details about this procedure are given in the section on development of an approximate term for constraint release and in the Appendix. Finally, the third step is to find the relaxation function of the Rouse tube:

$$R(t) = \left\langle \int_0^\infty \frac{dM}{d\varepsilon}\exp(-\varepsilon c_\nu t)\, d\varepsilon \right\rangle \tag{7}$$

where the brackets $\langle\ \rangle$ represent an average over different sets of mobilities that are distributed according to $P(\varepsilon)$. A dimensionless parameter, c_ν, is introduced to reflect the importance of the constraint-release mechanism. For example, when $c_\nu = 0$, there is no CR, whereas for $c_\nu = 1$, one constraint-release event occurs, and leads to an effective jump of the primary chain's tube by a distance equal to the tube diameter a. In other words, it is representative of the number of retraction events necessary to result in one tube hop of a tube diameter.[11]

The resulting material chain-relaxation function (without fast Rouse modes and longitudinal relaxation) is given by

$$G(t) = \frac{4}{5} G_e R(t)\mu(t) \tag{8}$$

where G_e is defined as the "entanglement" or elastic modulus:

$$G_e = \frac{\rho RT}{M_e} \tag{9}$$

Note that the experimentally observed plateau modulus $G_N^{(0)}$ is only 4/5 of G_e.

Material stress-relaxation function

To make the function $G(t)$ complete, one must still add the contributions from longitudinal stress relaxation

and fast Rouse modes. Combining all of the processes, the material stress-relaxation function takes the following form:

$$G(t) = G_e\left[\frac{4}{5}\,\mu(t)R(t) + \frac{1}{5Z}\sum_{p=1}^{Z-1}\exp\left(-\frac{p^2t}{\tau_R}\right) + \frac{1}{Z}\sum_{p=Z}^{N}\exp\left(-\frac{2p^2t}{\tau_R}\right)\right] \quad (10)$$

where the Rouse time $\tau_R = Z^2\tau_e$. The first term represents the contributions attributed to the escape from the tube (reptation and CLF) described by $\mu(t)$ and constraint release $R(t)$, the second term is longitudinal stress relaxation, and the third term is the fast Rouse motion inside the tube.

Monomer-dependent parameters

Monomer-dependent parameters are expected to vary with chemistry and monomer concentration, but not with molecular weight.[11] Three of these parameters have been discussed thus far:

(1) The elastic modulus G_e
(2) The Rouse time of an entanglement length τ_e
(3) The entanglement molecular weight M_e, which is related to the elastic modulus by eq. (9), $M_e = \rho RT/G_e$.

Note that in this work we are using the G definitions of the tube parameters as described by Larson et al.[13] and that the elastic modulus is larger than the experimentally observed plateau modulus by a factor of 5/4. These monomer-dependent parameters are difficult to measure experimentally, but they are present in all tube models that relate linear viscoelasticity and molecular structure, even for branched and polydisperse systems. Indeed, it would be interesting to derive them from simple rheological data by using an accurate model such as Likhtman–McLeish [eq. (10)]. This is not as simple as it appears and it is usually impossible to find a unique set of parameters that are optimal for a particular monomer chemistry. Here we attempt to remove some of this ambiguity by considering the zero-shear viscosity as well as the relaxation function.

There is an abundance of experimental data related to η_0 and its dependency on molecular weight. Because the integration of the material stress relaxation function [eq. (10)] with respect to time gives the zero-shear viscosity

$$\eta_0 = \int_0^\infty G(t)\,dt \quad (11)$$

it is possible to derive the monomer-dependent parameters by fitting the model to experimental data. For the Likhtman–McLeish model

$$\frac{\eta_0}{G_e\tau_e} = f(Z, c_\nu) \quad (12)$$

with three independent parameters (G_e, τ_e, and c_ν). To remove the dependency on the product $G_e\tau_e$, we can also look at the power law index α of the η_0 versus molecular weight relation [i.e., $(d \ln \eta_0)/(d \ln Z)$]. The relationship to experimental data comes from the well-known empirical relation[14]:

$$\eta_0 = K(Z_w)^\alpha \quad (13)$$

where $\alpha = 3.4$ over a wide range of molecular weights for most entangled polymers, and K is a function of temperature and monomer chemistry. Also, Z_w is the weight-average number of entanglements per chain in the case of polydisperse linear polymers and simply Z in the case of monodisperse linear polymers. Hence, it is possible to relate the theoretical α to available experimental data. We will see in the results section that this approach is partially successful in providing access to the monomer-dependent parameters.

DEVELOPMENT OF CLOSED-FORM SOLUTION FOR CONSTRAINT RELEASE

As mentioned previously, one of the primary goals of this work was to develop a closed-form representation of the constraint-release term $R(t)$, which is available only in stochastic form in the work of Likhtman and McLeish.[4] The stochastic term in eq. (7) is the spectrum of relaxation rates $dM/d\varepsilon$, which is determined by following the numerical procedure of Rubinstein and Colby.[5] We use the slightly modified procedure described in the Appendix to generate multiple realizations of the spectrum of relaxation rates for a broad range of Z and ultimately find average spectra for each Z. Finally, we fit a phenomenological equation to the results for all Z, thus providing a closed-form representation of $R(t)$ as below:

$$R(t) = \int_0^\infty \frac{d\bar{M}}{d\varepsilon}\exp(-\varepsilon c_\nu t)\,d\varepsilon \quad (14)$$

where $\bar{M}(\varepsilon) = \langle M(\varepsilon)\rangle$.

To find a representative average $M(\varepsilon) = \bar{M}(\varepsilon)$ it is necessary to generate spectra with many sets of random numbers at each Z (we used 25 realizations for the highest Z values and 235 realizations at the lowest Z values). In general the minimum acceptable number of realizations is that which provides a value of $\bar{M}(\varepsilon)$ that no longer changes when further realizations are added. Some examples of $\bar{M}(\varepsilon)$ are shown in Figure 1(a).

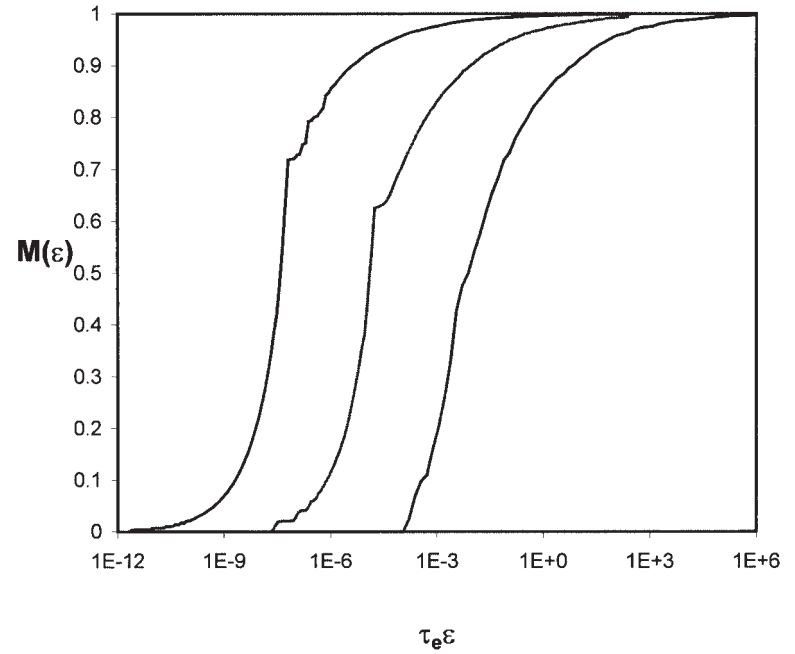

(a)

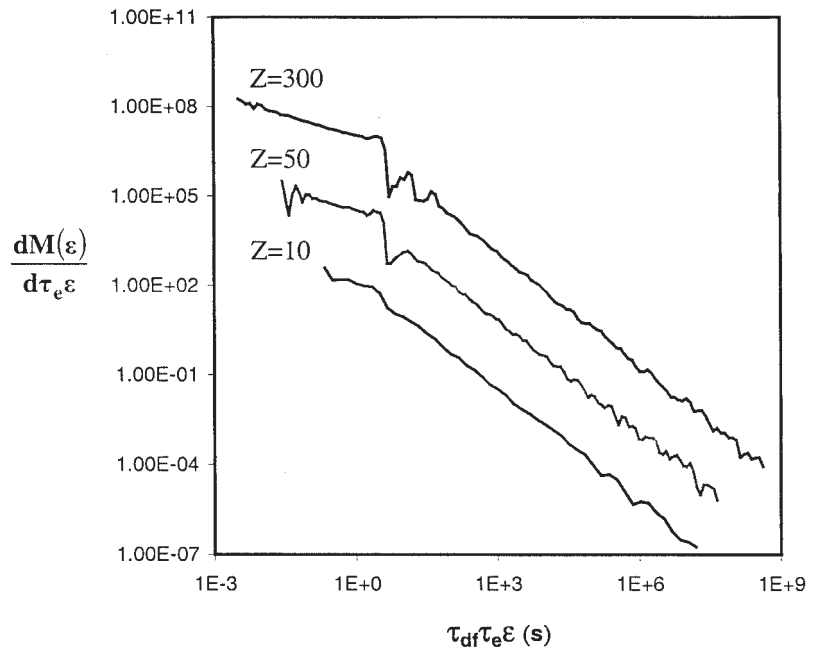

(b)

Figure 1 (a) Plot of $M(\varepsilon)$ for Z values of 10, 50, and 300. (b) Spectrum of normalized relaxation rates for Z values of 10, 50, and 300. The spectra are shifted horizontally by a factor of τ_{df} to illustrate the two regimes of this function that intersect at $\varepsilon = 1/\tau_{df}$.

Because the function that is actually required for $R(t)$ in eq. (14) is $d\bar{M}(\varepsilon)/d\varepsilon$ and the identification of the various regimes in this function is more straightforward than in $\bar{M}(\varepsilon)$, we fit the phenomenological model to $d\bar{M}(\varepsilon)/d\varepsilon$. Some examples of $d\bar{M}(\varepsilon)/d\varepsilon$ are shown in Figure 1(b). As shown in Figure 2, the gross behavior of this function can be represented by two power laws that intersect at $\varepsilon = 1/\tau_{df}$, given by eq. (15).

$$\frac{1}{\tau_e}\frac{d\bar{M}}{d\varepsilon} = \begin{cases} \exp(B_1)(\tau_e\varepsilon)^{-1/2} & \text{for } \varepsilon \le \dfrac{1}{\tau_{df}} \\ \exp(B_2)(\tau_e\varepsilon)^{-5/4} & \text{for } \varepsilon > \dfrac{1}{\tau_{df}} \end{cases} \tag{15}$$

In eq. (15) there are two parameters (B_1 and B_2) that are dependent on Z and τ_{df} and were determined by fitting simultaneously the $d\bar{M}(\varepsilon)/d\varepsilon$ curves resulting

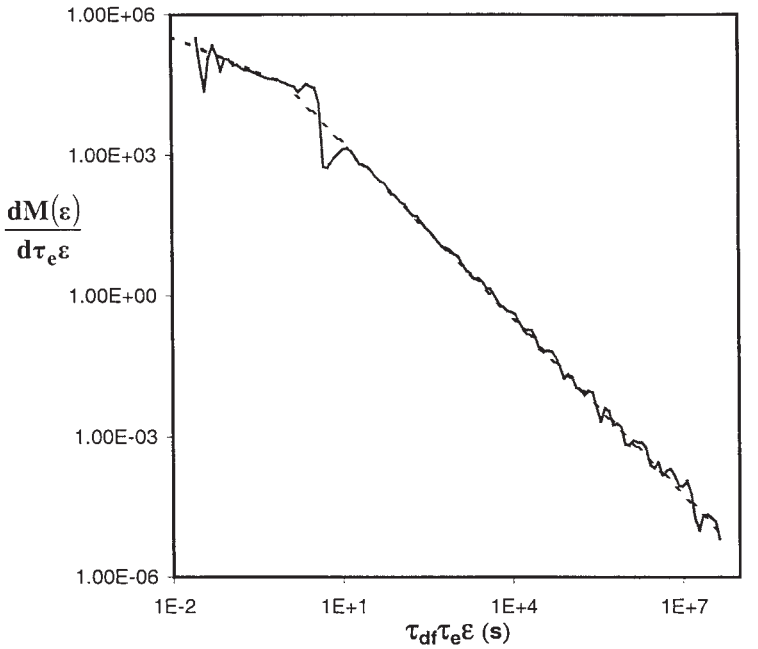

Figure 2 Spectrum of normalized relaxation rates for $Z = 50$ (solid line) and two power laws intersecting at $\varepsilon = 1/\tau_{df}$ (dashed line). For $\varepsilon < 1/\tau_{df}$, $dM/d\varepsilon \propto \varepsilon^{-1/2}$ and for $\varepsilon > 1/\tau_{df}$, $dM/d\varepsilon \propto \varepsilon^{-5/4}$.

from the stochastic simulations for Z values of 2, 10, 50, 75, 100, 150, 200, 250, and 300.

$$B_1 = \frac{3}{2}\ln(Z) - 1.63556$$
$$B_2 = \frac{3}{4}\ln\left(\frac{\tau_e}{\tau_{df}}\right) + B_1 \tag{16}$$

The gross behavior represented by eqs. (15) and (16) is insufficient to adequately capture the effect of constraint release on the material functions and it is also necessary to incorporate the sawtooth region that occurs at ε just greater than $1/\tau_{df}$. To do this it was necessary to develop the different models for different ranges of Z described below, all of which are encapsulated by the two power laws given in eq. (15). For $Z \leq 10$ there is no sawtooth function and eqs. (15) and (16) apply.

For $10 < Z \leq 160$, $d\bar{M}(\varepsilon)/d\varepsilon$ is given by the following equation:

$$\frac{1}{\tau_e}\frac{d\bar{M}}{d\varepsilon} = \begin{cases} \exp(B_1)(\tau_e\varepsilon)^{-1/2} & \text{for } \varepsilon \leq \dfrac{1}{\tau_{df}} \\ \exp(B_1)(\tau_e/\tau_{df})^{-1/2-n}(\tau_e\varepsilon)^n & \text{for } \dfrac{1}{\tau_{df}} < \varepsilon \leq \dfrac{2^2}{\tau_{df}} \\ 2^{2n-3}\exp(B_1-5)(\tau_e/\tau_{df})^{-2}(\tau_e\varepsilon)^{3/2} & \text{for } \dfrac{2^2}{\tau_{df}} < \varepsilon \leq \varepsilon_B \\ \exp(B_2)(\tau_e\varepsilon)^{-5/4} & \text{for } \varepsilon > \varepsilon_B \end{cases} \tag{17}$$

where B_1 and B_2 are given by eq. (16) and

$$\varepsilon_B = 2^{(-8n+12)/11}\exp\left(\frac{20}{11}\right)\left(\frac{1}{\tau_{df}}\right)$$
$$n = 0.161 \cdot (Z-10)^{0.2924} - 0.5$$

For $160 < Z \leq 360$, $d\bar{M}(\varepsilon)/d\varepsilon$ is given by the following equation:

$$\frac{1}{\tau_e}\frac{d\bar{M}}{d\varepsilon} = \begin{cases} \exp(B_1)(\tau_e\varepsilon)^{-1/2} & \text{for } \varepsilon \leq \dfrac{1}{\tau_{df}} \\ \exp(B_1)(\tau_e/\tau_{df})^{-1/2-n}(\tau_e\varepsilon)^n & \text{for } \dfrac{1}{\tau_{df}} < \varepsilon \leq \dfrac{2^2}{\tau_{df}} \\ 2^{2n-3}\exp(B_1-5)(\tau_e/\tau_{df})^{-2}(\tau_e\varepsilon)^{3/2} & \text{for } \dfrac{2^2}{\tau_{df}} < \varepsilon \leq \dfrac{4^2}{\tau_{df}} \\ 2^{2n-3}\exp(B_1-8)(\tau_e/\tau_{df})^{-2}(\tau_e\varepsilon)^{3/2} & \text{for } \dfrac{4^2}{\tau_{df}} < \varepsilon \leq \varepsilon_C \\ \exp(B_2)(\tau_e\varepsilon)^{-5/4} & \text{for } \varepsilon > \varepsilon_C \end{cases} \tag{18}$$

where B_1 and B_2 are given by eq. (16) and

$$\varepsilon_C = 2^{(-8n+12)/11}\exp\left(\frac{32}{11}\right)\left(\frac{1}{\tau_{df}}\right)$$
$$n = 0.161 \cdot (Z-10)^{0.2924} - 0.5$$

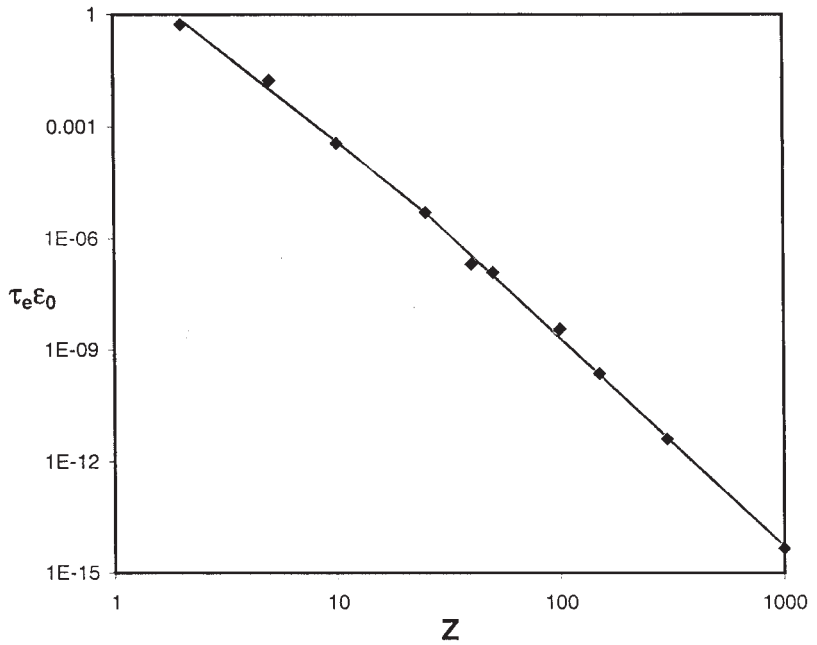

Figure 3 Comparison between eq. (20) (line) and the ε_0 values optimized according to eq. (19) (symbols).

For $Z > 360$ eq. (18) applies except the exponent n is 0.393, which corresponds to the value of n at $Z = 360$ in the preceding equation.

A final issue to be dealt with in the fitting of the relaxation rate spectrum is that of the lower limit in the integral of eq. (14). Our function for $d\bar{M}(\varepsilon)/d\varepsilon$ does not converge to a value of zero at low ε as it should so that $\lim_{\varepsilon\to\infty} \bar{M}(\varepsilon) = 1$. To ensure that the preceding limit is obeyed we define a lower limit for the integral in eq. (14), ε_0, such that the condition in eq. (19) is met:

$$\int_{\varepsilon_0}^{\infty} \frac{d\bar{M}}{d\varepsilon}\, d\varepsilon = 1 \tag{19}$$

This parameter was determined by nonlinear optimization for Z values of 5, 10, 25, 40, 50, 100, 150, 300, and 1000 and then correlated with Z as

$$\varepsilon_0 = \begin{cases} \dfrac{18.56Z^{-4.664}}{\tau_e} & Z < 25 \\ \dfrac{327.61Z^{-5.602}}{\tau_e} & Z \geq 25 \end{cases} \tag{20}$$

The quality of fit of eq. (20) is illustrated in Figure 3. It is worthwhile to note that the Z exponents are consistent with that of the maximum time in $R(t)$, which is proportional to $\tau_{df}Z^2$. In Figure 4(a)–(c) we demonstrate the quality of fit for the model for $d\bar{M}(\varepsilon)/d\varepsilon$ and its integral as compared to the stochastic results. In these figures we can see that the model for $d\bar{M}(\varepsilon)/d\varepsilon$ performs very well for the three representative data sets presented. The poorer fit of $\bar{M}(\varepsilon)$ is a result of small inaccuracies in eq. (20) for ε_0. As we show in the next section, these errors in ε_0 have a negligible effect on the material properties and therefore the use of a more complicated function in place of eq. (20) is not warranted.

RESULTS

Relaxation function of the Rouse tube $R(t)$

We presented earlier the relaxation function of the Rouse tube [eqs. (7) and (14)], which we now modify to incorporate the new limit on the integral:

$$R(t, c_\nu) = \left\langle \int_0^{\infty} \frac{dM}{d\varepsilon} \exp(-\varepsilon c_\nu t)\, d\varepsilon \right\rangle = \int_{\varepsilon_0}^{\infty} \frac{d\bar{M}}{d\varepsilon} \exp(-\varepsilon c_\nu t)\, d\varepsilon$$

where the average spectrum of relaxation rates $d\bar{M}(\varepsilon)/d\varepsilon$ is now expressed by eq. (15), (17), or (18), depending on Z.

In the previous section, comparisons were made between the stochastic simulations and the fitted $d\bar{M}(\varepsilon)/d\varepsilon$. At this point, $R(t)$ can be computed using

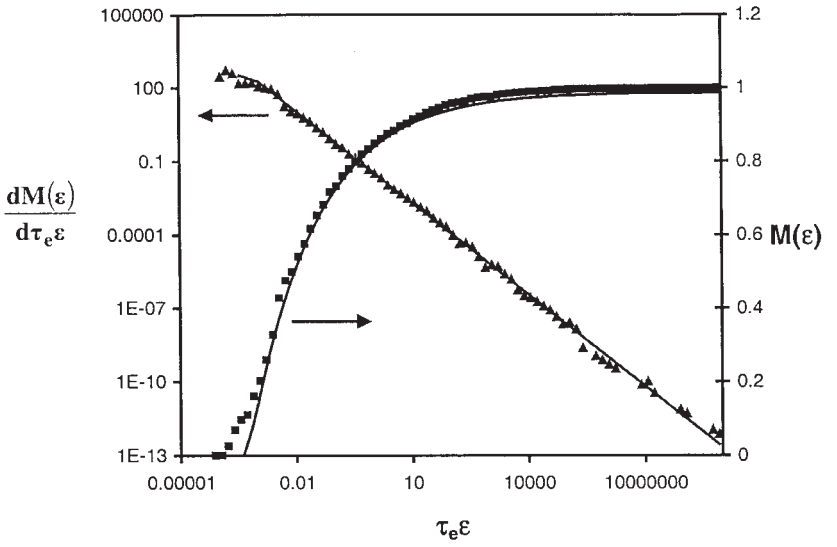

(a)

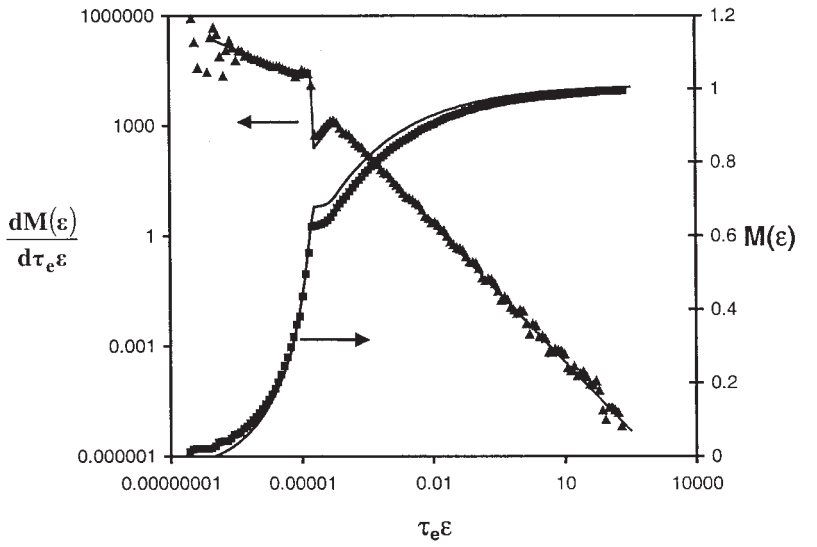

(b)

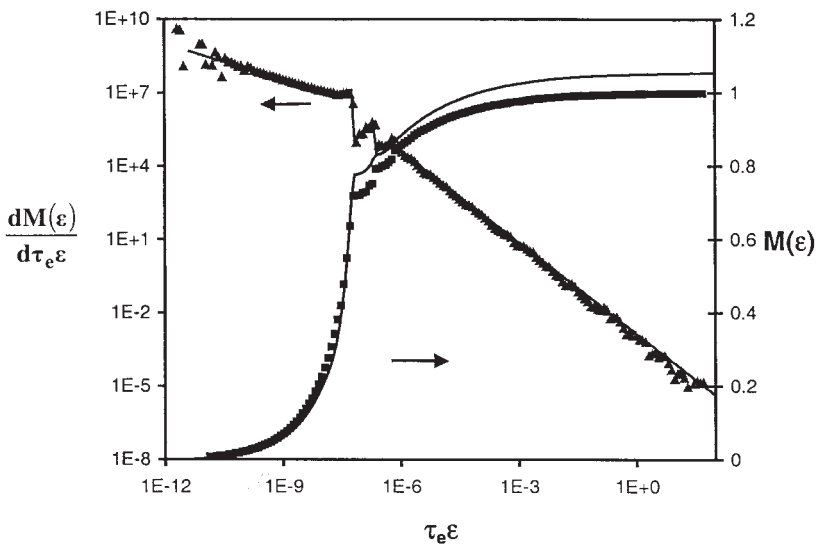

(c)

Figure 4 Comparison between stochastic results (symbols) and phenomenological model (lines) for (a) $Z = 10$, (b) $Z = 50$, and (c) $Z = 300$.

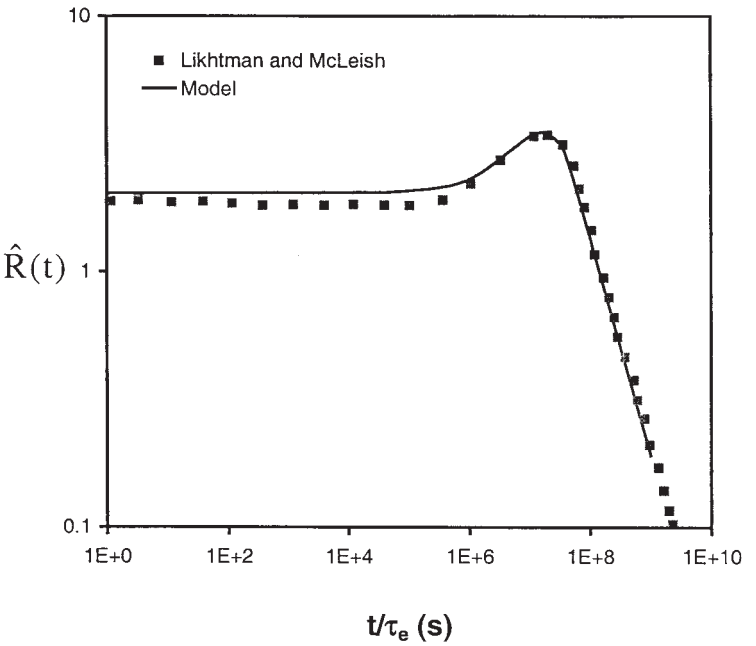

Figure 5 Normalized relaxation function of the Rouse tube, $\hat{R}(t)$, for $Z = 300$ and $c_\nu = 1$. Comparison between Likhtman and McLeish[4] data and present model.

the appropriate expression for $d\bar{M}(\varepsilon)/d\varepsilon$ and it becomes possible to compare the results of the closed-form equation with those of Likhtman and McLeish.[4] Their results for this function were presented in the form of

$$\hat{R}(t) = -4Z\tau_e^{1/4}t^{3/4}\frac{\partial R}{\partial t} \tag{21}$$

for $Z = 300$ and $c_\nu = 1$, as a function of normalized time in Figure 6 of Likhtman and McLeish.[4] The comparison between our results and theirs is presented in Figure 5. A small difference is observed at intermediate times, whereas the model performance is very good at long times. The limiting value at early times is estimated as 1.8 by Likhtman and McLeish[4] for $Z = 300$ and $c_\nu = 1$, whereas our value is 1.96. We will see later that the slight difference at early and intermediate times does not have a strong impact on the predictions of material properties.

To have more information on the performance our $d\bar{M}(\varepsilon)/d\varepsilon$ model, we also compared the normalized $R(t)$ obtained from our stochastic simulations with the one calculated from the phenomenological model for several other Z values. In Figure 6, we present a comparison for $Z = 100$ and $c_\nu = 1$. The model gives a good representation of the normalized $R(t)$ obtained from stochastic computations for all Z values studied in this work (up to $Z = 1000$).

Complex modulus G^*

Once we have a closed-form equation for the material relaxation function $G(t)$, it is possible to calculate the complex modulus G^*. As presented before, the relaxation function $G(t)$ is given by eq. (10):

$$G(t) = G_e\left[\frac{4}{5}\mu(t)R(t) + \frac{1}{5Z}\sum_{p=1}^{Z-1}\exp\left(-\frac{p^2t}{\tau_R}\right) + \frac{1}{Z}\sum_{p=Z}^{N}\exp\left(-\frac{2p^2t}{\tau_R}\right)\right]$$

The complex modulus G^* is a Fourier transformation of eq. (10):

$$G^*(\omega) = i\omega\int_0^\infty G(t)\exp(-i\omega t)\,dt \tag{22}$$

and

$$G^*(\omega) \equiv G'(\omega) + iG''(\omega) \tag{23}$$

where G' and G'' are the storage and loss moduli, respectively.

For $c_\nu = 0$ (i.e., constraint release removed), the normalized complex modulus takes the following form:

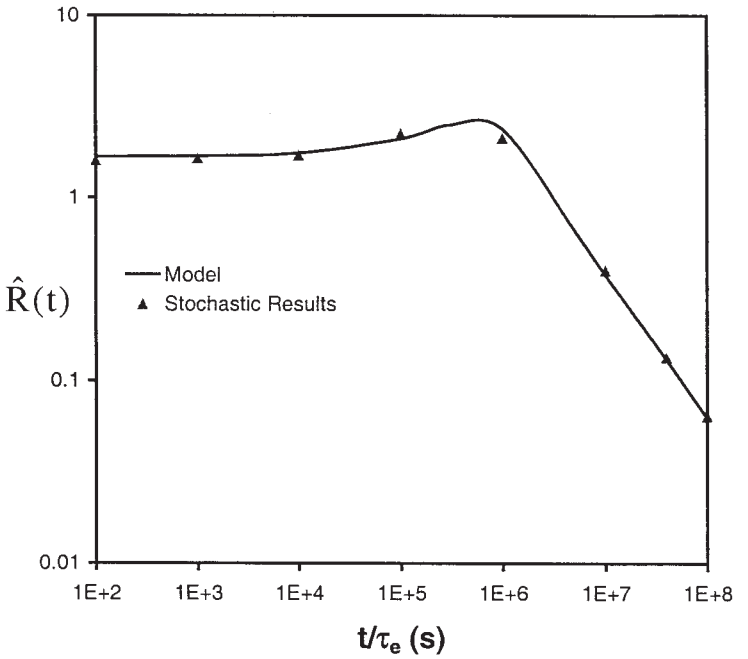

Figure 6 Normalized relaxation function of the Rouse tube, $\hat{R}(t)$, for $Z = 100$ and $c_\nu = 1$. Comparison between stochastic results and present model.

$$\frac{G^*(\omega)}{G_e} = \frac{32\omega\tau_{df}\tilde{G}_f}{5\pi^2}\sum_{p=1,\text{odd}}^{p^*}\frac{1}{p^2}\left[\frac{\omega\tau_{df} + i(p^2)}{(p^2)^2 + (\omega\tau_{df})^2}\right] + \left(\frac{4}{5}\right)\frac{0.306\omega}{Z\tau_e^{1/4}}\int_{\alpha^*}^{\infty}\frac{1}{\alpha^{5/4}}\left[\frac{\omega + i(\alpha)}{(\alpha)^2 + \omega^2}\right]d\alpha + \frac{\omega\tau_R}{5Z}\sum_{p=1}^{Z-1}\frac{\omega\tau_R + ip^2}{p^4 + (\omega\tau_R)^2} + \frac{\omega\tau_R}{Z}\sum_{p=Z}^{N}\frac{\omega\tau_R + i2p^2}{4p^4 + (\omega\tau_R)^2} \quad (24)$$

whereas for $c_\nu > 0$, $G^*(\omega)/G_e$ is given by

$$\frac{G^*(\omega)}{G_e} = \frac{32\omega\tau_{df}\tilde{G}_f}{5\pi^2}\sum_{p=1,\text{odd}}^{p^*}\frac{1}{p^2}\int_{\varepsilon_0}^{\infty}\frac{d\bar{M}}{d\varepsilon}\left[\frac{\omega\tau_{df} + i(p^2 + \varepsilon c_\nu\tau_{df})}{(p^2 + \varepsilon c_\nu\tau_{df})^2 + (\omega\tau_{df})^2}\right]d\varepsilon + \left(\frac{4}{5}\right)\frac{0.306\omega}{Z\tau_e^{1/4}}\int_{\alpha^*}^{\infty}\frac{1}{\alpha^{5/4}} \times \int_{\varepsilon_0}^{\infty}\left[\frac{\omega + i(\alpha + \varepsilon c_\nu)}{(\alpha + \varepsilon c_\nu)^2 + \omega^2}\right]\frac{d\bar{M}}{d\varepsilon}d\varepsilon d\alpha + \frac{\omega\tau_R}{5Z}\sum_{p=1}^{Z-1}\frac{\omega\tau_R + ip^2}{p^4 + (\omega\tau_R)^2} + \frac{\omega\tau_R}{Z}\sum_{p=Z}^{N}\frac{\omega\tau_R + i2p^2}{4p^4 + (\omega\tau_R)^2} \quad (25)$$

which contains, of course, $d\bar{M}(\varepsilon)/d\varepsilon$. The moduli G' and G'' are obtained from the respective real and imaginary parts of eq. (24) or (25).

In Figures 7(a) and (b), we present normalized storage and loss moduli, respectively, as a function of normalized frequency, for $c_\nu = 1$ and Z values of 2, 25, 100, 300, and 1000. Our calculations were performed using the fitted $d\bar{M}(\varepsilon)/de$. The comparison between the results of Likhtman and McLeish[4] and the model with our fitted equations for constraint release is excellent. This confirms that the fit of $d\bar{M}(\varepsilon)/d\varepsilon$ is appropriate to estimate correctly the material functions.

Limiting low rate viscosity η_0

The limiting low rate or zero-shear viscosity η_0 can also be obtained by the appropriate integration of the relaxation material function $G(t)$ [eq. (10)], as presented in eq. (11):

$$\eta_0 = \int_0^{\infty} G(t)\,dt$$

For the case without constraint release ($c_\nu = 0$), the zero-shear viscosity is expressed as

$$\frac{\eta_0}{G_e} = \frac{4}{5}\frac{8\tilde{G}_f}{\pi^2}\sum_{p=1,\text{odd}}^{p^*}\frac{\tau_{df}}{p^4} + \frac{16}{25}\frac{0.306}{Z\tau_e^{1/4}(\varepsilon^*)^{5/4}} + \frac{\tau_R}{5Z}\sum_{p=1}^{Z-1}\frac{1}{p^2} + \frac{\tau_R}{2Z}\sum_{p=Z}^{N}\frac{1}{p^2} \quad (26)$$

whereas for $c_\nu > 0$, it is given by

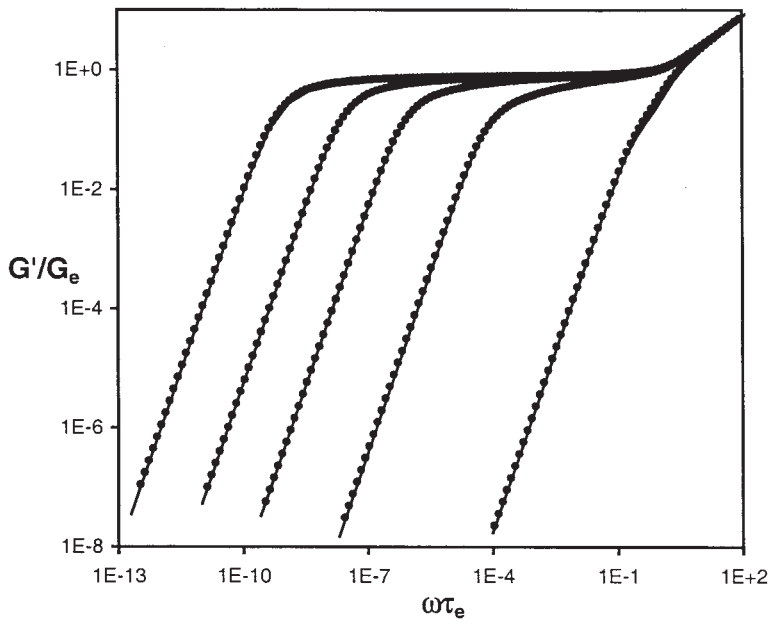

(a)

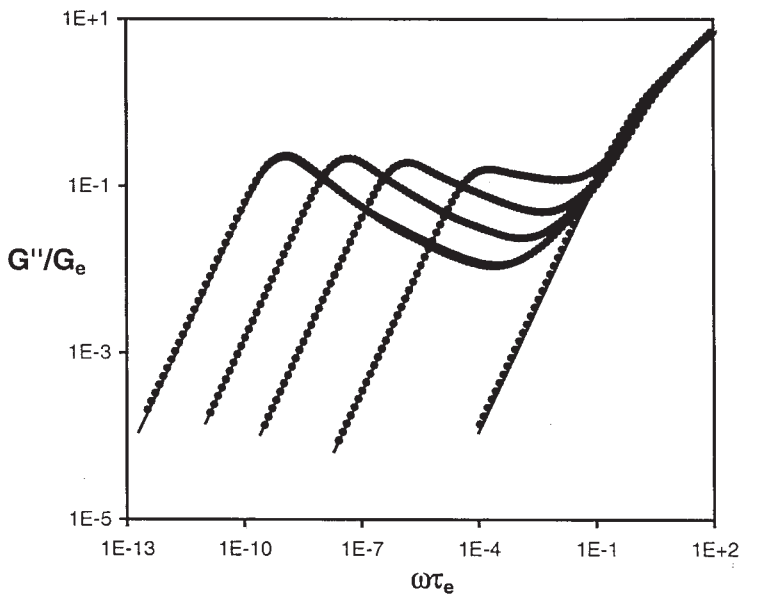

(b)

Figure 7 (a) Prediction of normalized storage moduli G' and (b) of normalized loss module G″ for $c_\nu = 1$ and Z values of 2, 25, 100, 300, and 1000. Symbols represent data from Likhtman and McLeish[4]; lines represent predictions from the present model.

$$\frac{\eta_0}{G_e} = \frac{4}{5}\frac{8\tilde{G}_f}{\pi^2}\sum_{p=1,\text{odd}}^{p^*}\frac{1}{p^2}\int_{\varepsilon_0}^{\infty}\frac{d\bar{M}}{d\varepsilon}\frac{1}{\dfrac{p^2}{\tau_{df}}+\varepsilon c_\nu}\,d\varepsilon + \frac{4}{5}\frac{0.306}{Z\tau_e^{1/4}}\int_{\varepsilon^*}^{\infty}\int_{\varepsilon_0}^{\infty}\frac{1}{\alpha^{5/4}}\frac{d\bar{M}}{d\varepsilon}\frac{1}{\alpha+\varepsilon c_\nu}\,d\varepsilon d\alpha + \frac{\tau_R}{5Z}\sum_{p=1}^{Z-1}\frac{1}{p^2}+\frac{\tau_R}{2Z}\sum_{p=Z}^{N}\frac{1}{p^2} \quad (27)$$

which again contains $d\bar{M}(\varepsilon)/d\varepsilon$. The last two terms in eqs. (26) and (27) may be approximated, as shown below, with minimal impact for $Z > 4$.

$$\frac{\tau_R}{5Z}\sum_{p=1}^{Z-1}\frac{1}{p^2}\cong\frac{\pi^2\tau_R}{60Z}\left(2-\frac{1}{Z-1}\right)\times\frac{\tau_R}{2Z}\sum_{p=Z}^{N}\frac{1}{p^2}\cong\frac{\tau_R}{2Z^2} \quad (28)$$

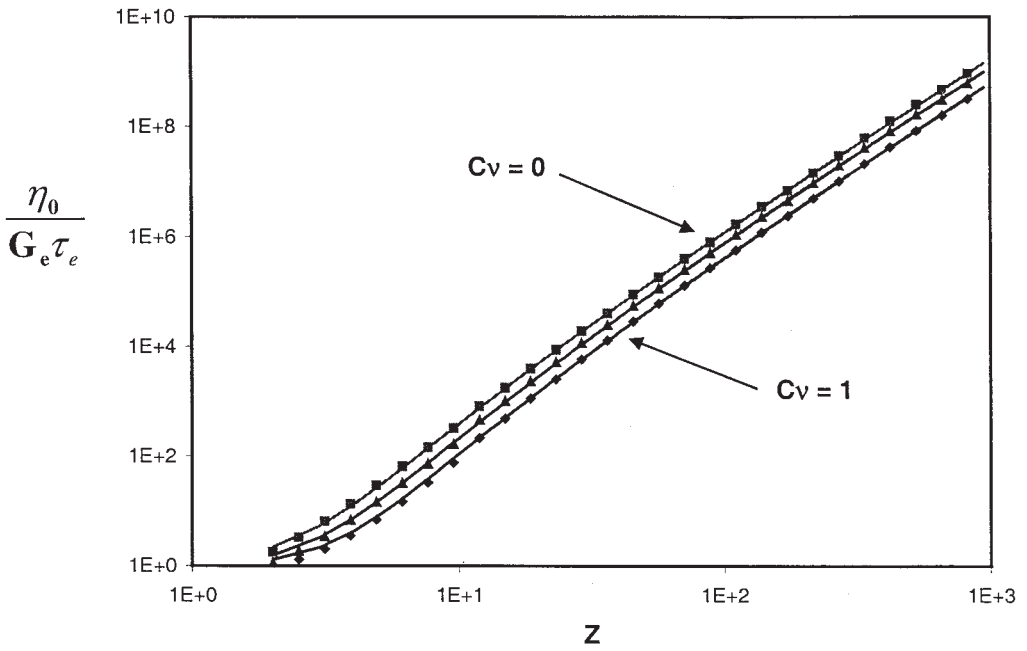

Figure 8 Prediction of normalized zero-shear viscosity η_0 for c_ν values of 0, 0.1, and 1. Lines represent data from Likhtman and McLeish[4]; symbols represent predictions from the present model.

In Figure 8, we compare computed normalized zero-shear viscosity with the results of Likhtman and McLeish[4], for c_ν values of 0, 0.1, and 1. Again, we used the fitted form of $d\bar{M}(\varepsilon)/d\varepsilon$ to obtain our values. Excellent agreement is obtained for $Z > 5$. For $2 < Z < 5$, the viscosity is slightly underestimated.

As mentioned earlier, another interesting way to compare η_0 experimental data with theoretical predictions is by examining the power-law exponent $\alpha = (d \ln \eta_0)/(d \ln Z)$, which eliminates the dependency on the product $G_e\tau_e$, leaving only Z and c_ν as parameters. In Figure 9, we compare the α-values calculated with our $d\bar{M}(\varepsilon)/d\varepsilon$ with those of Likhtman and McLeish,[4] which we found by numerically differentiating their zero-shear viscosity data. For our model, the slope of the $c_\nu = 0$ case was obtained by the numerical differentiation of eq. (26), whereas for $c_\nu = 1$, we differentiated eq. (27). As expected, for $c_\nu = 0$, the agreement with Likhtman and McLeish[4] data is excellent, and we therefore show only our results in Figure 9. For $c_\nu = 1$ we observe several oscillations in the α obtained with the closed-form $d\bar{M}(\varepsilon)/d\varepsilon$ equation. The maximum

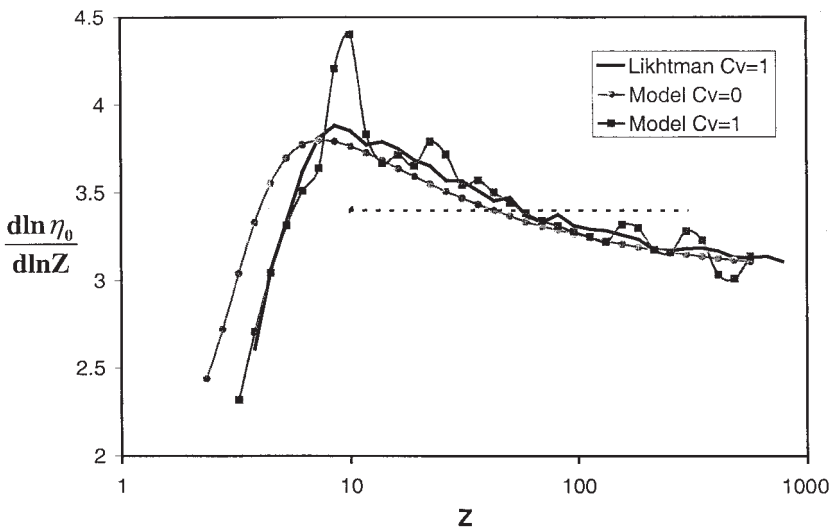

Figure 9 Comparison of the slope of the zero-shear viscosity versus molecular weight for $c_\nu = 0$ and $c_\nu = 1$. The dotted line represents the empirical value of 3.4.

around $Z = 10$ is attributed to the fact that we started to incorporate sawtooth functions for $Z > 10$ in $d\bar{M}(\varepsilon)/d\varepsilon$ [eqs. (20) and (21)]. These functions create oscillations in $(d \ln \eta_0)/(d \ln Z)$ and a maximum at the point of incorporation. The peak deviation with Likhtman–McLeish data is observed at Z slightly larger than 10, with a 14% deviation. Elsewhere, the oscillations result in a difference of about 3–4%. Nevertheless, the initial part of the slope is the same, and the overall shape and values are similar to those of Likhtman and McLeish.[4] We shall then use our model to calculate the zero-shear viscosity to make comparisons with experimental data, and we will use the Likhtman–McLeish data for calculating $(d \ln \eta_0)/(d \ln Z)$ as will be seen in the next section. One final remark is concerning the dotted line in Figure 9, which represents the empirical value of 3.4 over the experimental range of molecular weight generally used. We should keep in mind that this comparison is made between an average value (dotted line) and the instantaneous calculated values.

Comparison with experimental data

In their work, Likhtman and McLeish[4] present a detailed comparison of theoretical predictions of G' and G'' with experimental data for two sets of polystyrene (PS) and polybutadiene (PB). They use τ_e and G_e as fitting parameters (identical for all samples of fixed monomer chemistry), and use eq. (9) to calculate M_e. They also set $c_\nu = 1$. In both cases of PS data, the agreement is very reasonable. However, in the case of PB, the quality of fit is unacceptable: G' is underestimated in the intermediate regime, and the terminal zones are not fitted correctly. Improvement can be obtained if they consider G_e and M_e as independent parameters. However, this leads to a product G_eM_e higher by 50–60% than predicted by eq. (9). One of their conclusions is that PS is described very well by the theory, but that PB shows problems and that more high-precision data are needed to confirm this disagreement, which may be a first indication of nonuniversality of polymer dynamics.[4]

In our work, comparisons are focused on zero-shear viscosity data for nearly monodisperse polyethylene (PE) and PS. To do so, the monomer-dependent and constraint-release parameters must be known or fitted with sets of data of fixed monomer chemistry. Unfortunately, reliable experimental values of monomer-dependent parameters are sparse in the literature. Furthermore, the constraint-release parameter c_ν has rarely been mentioned, except for the Likhtman and McLeish[4] and Graham et al.[11] works where c_ν values of 1 and 0.1 were used, respectively.

For nearly monodisperse PE (or its near equivalent, hydrogenated polybutadiene), most references report values in the range of 828 to 1390 g/mol for the entanglement molecular weight M_e.[15–20] Most of these values are derived from a measurement of the experimental plateau modulus $G_N^{(0)}$ and the use of eq. (9), assuming that the elastic modulus and the plateau modulus are the same. In fact, according to Likhtman and McLeish,[4] a more appropriate relationship between the plateau modulus and the entanglement molecular weight is given by eq. (29). In the literature values for M_e only the lowest are based on eq. (29)[15]:

$$G_N^{(0)} = \frac{4}{5}\frac{\rho RT}{M_e} \tag{29}$$

The monomeric friction coefficient ζ, which determines the elementary time τ_e, is more complex to determine than the plateau modulus, and it is extremely difficult to find reliable data about it in the literature. Therefore we are left with two unknown parameters, c_ν for constraint release and τ_e, which also contains the temperature dependency. It is useful to exploit the simulations and some experimental data for the zero-shear viscosity to determine τ_e. In a first approach, we use measurements for PE with $Z < 2$, where only the fast Rouse motion is active. In this case, the zero-shear viscosity is determined solely by the last term of eq. (26). One reference[21] containing many sets of data for nearly monodisperse PE (hydrogenated polybutadiene) was considered here, where measurements were performed for $M_w = 1050$ g/mol. They found the plateau modulus to be 2.3 MPa, or $G_e = 2.88$ MPa at $T = 448$ K. Using the density presented by Fetters et al.[15] for PE, we calculate M_e to be 1000 g/mol, which is in the range of the values presented above. For $Z = 1.05$, the measured zero-shear viscosity is 0.0064 Pa s^{-1} at $T = 448$ K.[21] Combined with theoretical predictions we find $\tau_e = 2.6 \times 10^{-9}$ s at $T = 448$ K. We can now plot the zero-shear viscosity for all M_w values normalized by the product $G_e\tau_e = 7.5 \times 10^{-3}$ Pa s^{-1} and determine which c_ν value best represents the PE data.

The comparison for molecular weights ranging between 2510 and 959,000 g/mol[21] is shown in Figure 10. Error bars correspond to 10% uncertainty in molecular weight (x-axis) and 5% in viscosity (y-axis) (smaller than symbols). As one may observe no single value of c_ν adequately represents the data of PE. The best compromise is $c_\nu = 0.1$, as suggested by Graham et al.[11] as a universal value, considering that entangled polymers are governed by universal underlying dynamics. The value of $c_\nu = 0.1$ is also close to the value derived by Schieber[22] ($c_\nu = 1/12$), in his work using a slip-link model that includes consistent constraint release, also inspired by the ideas of Rubinstein and Colby.[5]

In the case of PS, many references report values of the entanglement molecular weight M_e between 18,100 and 18,900 g/mol.[3,15–17,20] Again, it is most probable

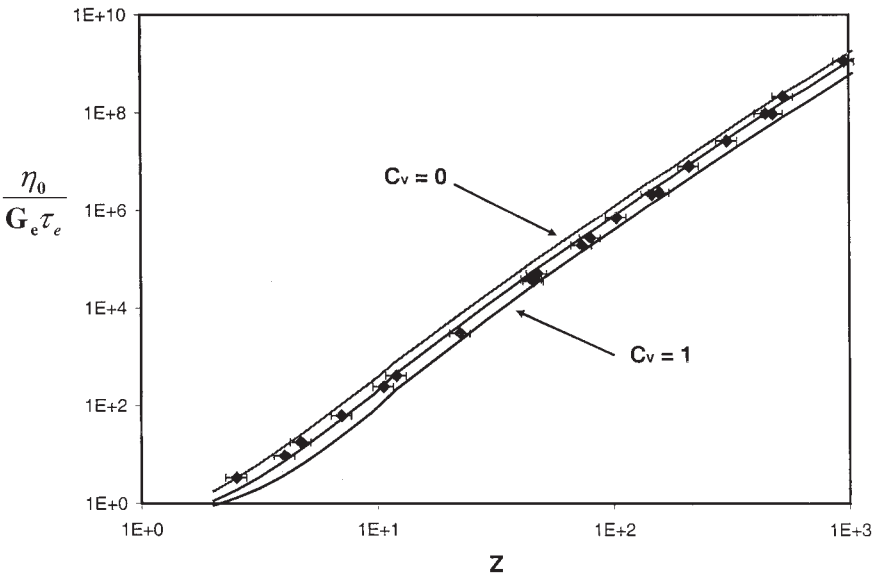

Figure 10 Normalized zero-shear viscosity of PE shifted with product $G_e\tau_e$ = 7.5E-3 Pa s^{-1}. Symbols represent experimental data (Pearson et al.[21]). Error bars correspond to 10% uncertainty in molecular weight (x-axis) and 5% in viscosity (y-axis) (smaller than symbols).

that the factor 4/5 was not used to evaluate M_e [eq. (29)], except for the lowest value recorded (13,309 g/mol), which is from the same work that reported the lowest value of M_e for PE.[15] In a first approach, we follow a procedure similar to that for PE (i.e., using data for $Z < 2$ to determine τ_e). This time, a data set[23] with several values is available for that low range of Z values and we can therefore obtain more reliable information than for PE, for which only one molecular weight was available. For Z values ranging between 0.639 and 1.74, the calculated product $G_e\tau_e$ varies considerably, as shown in Table I. We used the average value of this product (34 Pa s^{-1}) to shift the PS data from Majeste et al.[23] and Schausberger et al.[24] The results are shown in Figure 11. As for PE, again no single c_ν gives an adequate fit and a value of 0.1 could be a compromise.

TABLE I
Calculation of the Product $G_e\tau_e$ for Polystyrene in the Low-Z Regime ($Z < 2$)[a]

M_w (g/mol)	Z[b]	η_0 (453 K)[c] (Pa s^{-1})	$G_e\tau_e$ (Pa s^{-1})	τ_e[d] (s)
9.20E+03	6.39E-01	1.17E+01	22.5	9.0E-05
1.02E+04	7.08E-01	1.00E+01	17.3	6.9E-05
1.30E+04	9.03E-01	2.14E+01	28.9	1.2E-04
1.57E+04	1.09E+00	3.78E+01	42.4	1.7E-04
1.62E+04	1.13E+00	3.00E+01	32.5	1.3E-04
1.75E+04	1.22E+00	4.57E+01	45.9	1.8E-04
2.02E+04	1.40E+00	2.81E+01	24.4	9.8E-05
2.50E+04	1.74E+00	8.71E+01	61.1	6.3E-04

[a] Experimental data are from Majeste et al.[22]
[b] Calculated using a value of M_e = 14,400 g/mol.
[c] Data shifted from 433 K using the shift factor of Schausberger et al.[23]
[d] Calculated using a value of G_e = 2.5E+05 Pa.

It is interesting to note that, as expected, the product $G_e\tau_e$ obtained for PS results in a much larger elementary time τ_e than that for PE. Using the plateau modulus of 2×10^5 Pa at 463 K[17] (the same value has been reported at 413 K[15]), we determine G_e to be 2.5×10^5 Pa. Using a density of 959 kg/m^3[20] for PS, we calculate M_e to be 14,400 g/mol. This value is used to calculate the Z values. The relaxation time τ_e is of the order of 10^{-4} s, whereas it was 10^{-9} s for PE. All the monomer-dependent parameters values determined here with zero-shear viscosity data for PS are in agreement with those fitted by Likhtman and McLeish[4] in their comparison with complex moduli experimental data. For one set of PS data,[24] they determined $G_e = 2.79 \times 10^5$ Pa, $\tau_e = 3.36 \times 10^{-4}$ s, and M_e = 12,960 g/mol, at T = 453 K, and for another set of data,[25] they calculated $G_e = 2.69 \times 10^5$ Pa, $\tau_e = 9.22 \times 10^{-4}$ s, and M_e = 14,470 g/mol, at T = 442.5 K.

In Figure 12, we compare the $(d \ln \eta_0)/(d \ln Z)$ calculated from the experimental data of PE and PS with those obtained from the Likhtman and McLeish[4] results for zero-shear viscosity. We use their results in this application because of the spurious oscillations introduced into the derivation by the new model for $d\bar{M}(\varepsilon)/d\varepsilon$. The data are sparse and, as was seen with the viscosity itself, it is difficult to discriminate which constraint-release parameter best represents the experimental data for both materials, although this approach seems to indicate that a value close to 1 is appropriate at low and high Z values. The peak calculated by the Likhtman–McLeish model[4] is not in

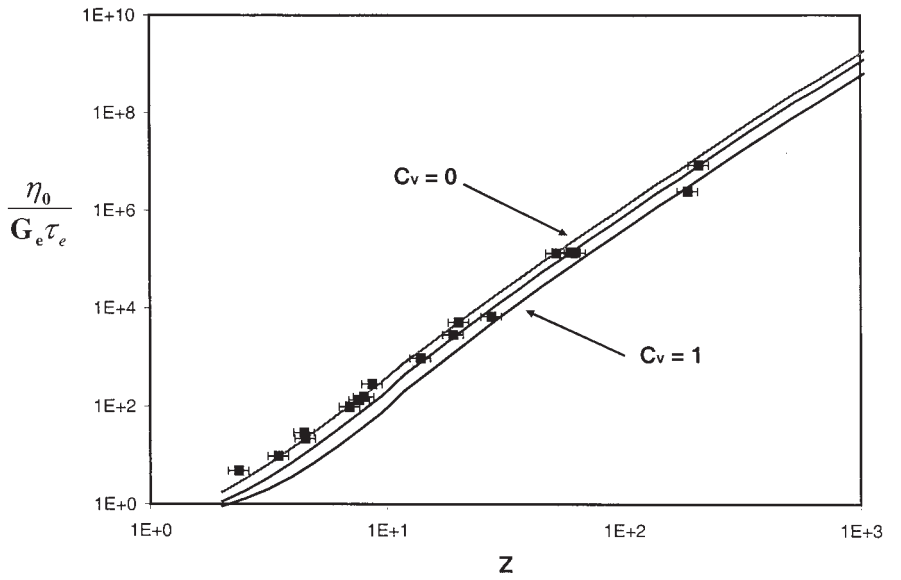

Figure 11 Normalized zero-shear viscosity of PS shifted with product $G_e\tau_e = 34$ Pa s^{-1}. Symbols represent experimental data (Majeste et al.[23] and Schausberger et al.[24]). Error bars correspond to 10% uncertainty in molecular weight (x-axis) and 5% in viscosity (y-axis) (smaller than symbols).

agreement with experimental data, but the overall model predictions are in the right range. This is a clear improvement from the original tube models, which could not predict a power-law exponent > 3. We should, however, note that the model approaches 3 at high molecular weights, which is not clear in the experimental data.

DISCUSSION

The presence of the constraint-release parameter c_ν complicates the determination of the monomer-dependent parameters from experimental data if they are unknown, which is unfortunately most often the case. The approach of Likhtman and McLeish[4] to set $c_\nu = 1$ did not give acceptable results for our computations of zero-shear viscosity of PE and PS. The value of $c_\nu = 0.1$ proposed by Graham et al.[11] seemed more appropriate. We believe that a valuable approach is to determine the monomer chemistry–dependent parameters from results for unentangled polymers, thus removing the complication of constraint release. Then, entangled polymer data can be used to determine the best value of c_ν. However, there may be shifts in the glass tran-

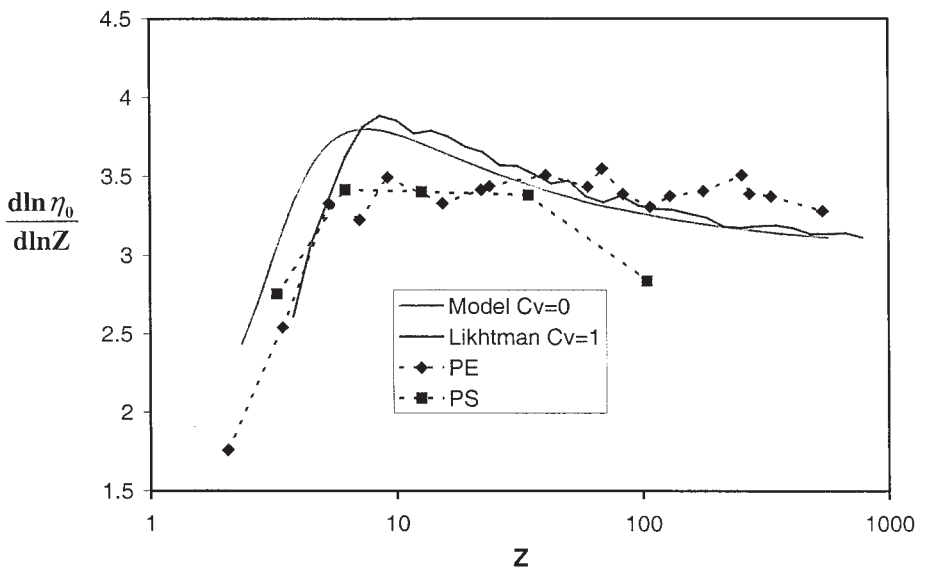

Figure 12 Comparison of the calculated slope of the zero-shear viscosity versus molecular weight for $c_\nu = 0$ and $c_\nu = 1$ with experimental data for PE (Pearson et al.[21]) and PS (Majeste et al.[23] and Schausberger et al.[24]).

sition of low molecular weight chains, resulting from chain ends, which can cause a complication in determination of the parameters if many sets of data at various molecular weights are used. Furthermore, it is possible that the slight amount of polydispersity, contained in all polymers, complicates the analysis. All these factors might partly account for the deviations between experiment and theory.

Obviously, the scatter in the experimental data makes it difficult to determine the value of c_ν precisely, even when the monomer-dependent parameters are known. In this work, a compromise value of $c_\nu = 0.1$ is used for PE, but no single value really fits all of the zero-shear viscosity data. Instead it appears that at very low Z a lower value of c_ν is more appropriate and at intermediate Z a higher c_ν value is required. At $Z > 200$ the required c_ν decreases again. Similarly, the PS data indicate that a constraint-release parameter that depends on Z could improve the fit with c_ν increasing from low to intermediate Z. However, the experimental data end at Z approximately equal to 200 and we therefore do not see the decrease of the required c_ν that we saw with PE. If this observation is real, then it indicates that higher molecular weight chains are affected to a greater degree by constraint release; that is, a single constraint-release event corresponds to larger jumps in the primary chain's tube for higher molecular weights. However, this would be in contradiction with the concept of a universal value of c_ν, considering universal underlying dynamics for the behavior of entangled polymers.[11]

The most obvious disagreement between the model prediction and zero-shear viscosity experimental data resides in the power-law exponent $(d \ln \eta_0)/(d \ln Z)$ versus molecular weight. The predicted peak at intermediate values of Z is not physical, given that the experimental exponents seen here for PE and PS are almost flat. However, the prediction of the exponent at low and high Z values is much better.

Our experience with the Likhtman–McLeish model leads us to conclude that it is a definite improvement over previous theoretical models, both in the prediction of complex moduli and zero-shear viscosity. However, in its original version it is very computationally intensive, except for computations at short times ($t < \tau_R$) for which an analytical solution is presented for the relaxation function $R(t)$. Therefore, it is not readily usable without access to the source code. The approximate closed-form solution proposed here, valid at all times, should enable a wider use of the model. Indeed, even with the inherent difficulties in simultaneously determining the best values of all parameters from experimental data, and the remaining disagreement with experimental observations for $(d \ln \eta_0)/(d \ln Z)$, this model represents a very useful tool for the prediction of experimental data of entangled linear homopolymers in the linear viscoelastic region, or for the approximate evaluation of monomer-dependent parameters.

CONCLUSION

In this work, we present an approximate closed-form representation of the Likhtman–McLeish model, which is valid at all times and simplifies its use. In addition, analytical integration of the material relaxation function $G(t)$ was performed to obtain an expression for the zero-shear viscosity. Results of the computations of the zero-shear viscosity were compared with available experimental data for monodisperse entangled linear PE and PS. The model is considered a major improvement over previous theoretical models, both in the prediction of complex moduli[4] and zero-shear viscosity, even if there is still some disagreement between the predictions and experimental data of the slope $(d \ln \eta_0)/(d \ln Z)$ versus molecular weight. The main difficulty in using this model resides in the simultaneous fit of the monomer-dependent and constraint-release parameters. It is however considered a useful tool for the prediction of experimental data of entangled linear homopolymers in the linear viscoelastic regime, or for the approximate evaluation of monomer-dependent parameters.

The authors gratefully acknowledge the helpful comments of A. Likhtman and the reviewer.

APPENDIX

Numerical procedure for generating the spectrum of relaxation rates

We use a slightly modified version of the procedure described by Rubinstein and Colby.[5] The first step in the numerical procedure is to generate a set of Z mobilities m_i that follow the probability distribution $P(\varepsilon)$. We do this by the cumulative probability distribution, $CP(\varepsilon)$, which is given in general by eq. (A.1) and specifically for the theory considered here by eq. (A.2).

$$CP(\varepsilon) = \int_0^\varepsilon P(\varepsilon)\, d\varepsilon = \int_0^\varepsilon \mathcal{L}^{-1}\{\mu(t)\}\, d\varepsilon \qquad \text{(A.1)}$$

In eq. (A.1) $\mathcal{L}^{-1}\{\}$ indicates the inverse Laplace transform, t is the Laplace domain variable, and ε is the inverse Laplace domain variable. Note that eq. (A.1) is simply the definition of a cumulative probability distribution applied to the differential probability distribution in eq. (6). By substituting eq. (1) for $\mu(t)$ into eq. (A.1) and then performing the inverse Laplace transform we produce eq. (A.2):

$$CP(\varepsilon) = CP_1(\varepsilon) + CP_2(\varepsilon)$$

where

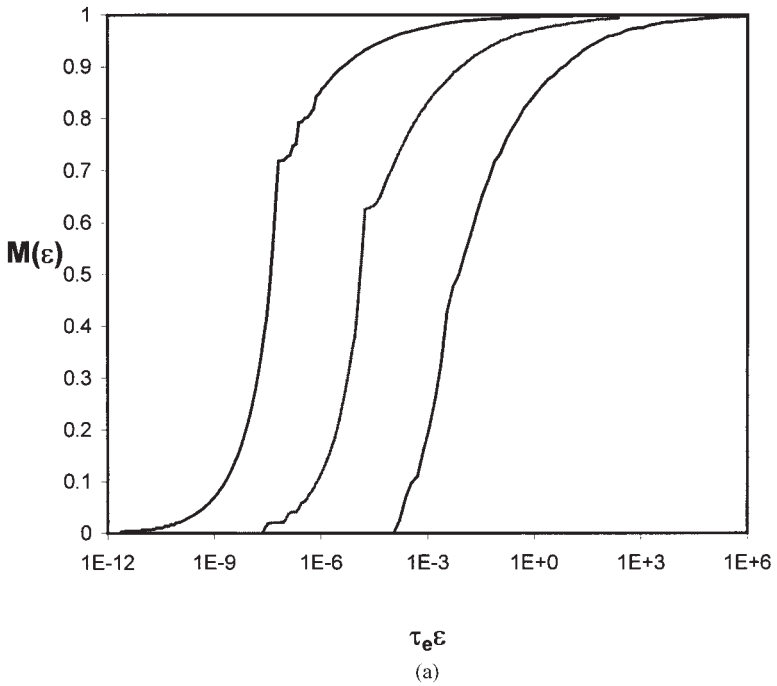

Figure A.1 Cumulative probability distribution [eq. (A.2)] for $Z = 300$. The steps correspond to the reptation modes and the curved portions correspond to CLF.

$$CP_1(\varepsilon) = \frac{8\tilde{G}_f}{\pi^2}\begin{cases} 0 & \varepsilon < \dfrac{1}{\tau_{df}} \\ \displaystyle\sum_{\substack{p=1 \\ odd}}^{\sqrt{\varepsilon\cdot\tau_{df}}} \frac{1}{p^2} & \dfrac{1}{\tau_{df}} \le \varepsilon < \dfrac{(p^*)^2}{\tau_{df}} \\ \displaystyle\sum_{\substack{p=1 \\ odd}}^{p^*} \frac{1}{p^2} & \varepsilon \ge \dfrac{(p^*)^2}{\tau_{df}} \end{cases}$$

and

$$CP_2(\varepsilon) = 4\left(\frac{0.306}{Z\tau_e^{1/4}}\right)\begin{cases} 0 & \varepsilon < \varepsilon^* \\ \dfrac{1}{(\varepsilon^*)^{1/4}} - \dfrac{1}{(\varepsilon)^{1/4}} & \varepsilon \ge \varepsilon^* \end{cases} \qquad \text{(A.2)}$$

In eq. (A.2), the cumulative probability function $CP_1(\varepsilon)$ corresponds to the reptation term in $\mu(t)$ and

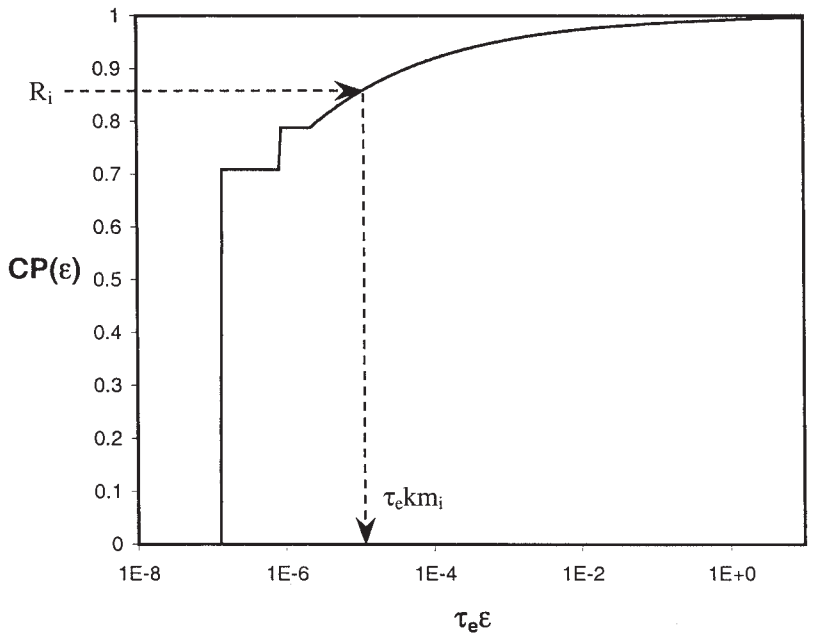

Figure A.2 Demonstration of generation of reduced mobilities, $Z = 150$.

$CP_2(\varepsilon)$ corresponds to the CLF term. The cumulative probability distribution for $Z = 300$ is shown in Figure A.1.

Next, Z random numbers R_i between 0 and 1 are generated and the corresponding km_i are found, as indicated on Figure A.2 for $Z = 150$. This procedure results in a set of reduced mobilities (with dimensions of inverse time) that follow the probability distribution $P(\varepsilon)$.

The next step is to solve the following set of recursive equations. The fraction of negative S_i at a particular ε is $M(\varepsilon)$[4,5]:

$$S_i = km_i + km_{i+1} - \varepsilon - \frac{(km_i)^2}{S_{i-1}} \quad \text{for } 2 \le i \le Z - 1$$

$$S_1 = km_1 + km_2 - \varepsilon \tag{A.3}$$

where k, the elastic constant of the sections of the chains, is equal to $3k_BT/a^2$. For more details about this calculation see Rubenstein and Colby.[5]

References

1. deGennes, P. G. J Chem Phys 1971, 55, 572.
2. Doi, M.; Edwards, S. F. The Theory of Polymer Dynamics; Clarendon: Oxford, UK, 1986.
3. Ferry, J. D. Viscoelastic Properties of Polymers, 2nd ed.; Wiley: New York, 1970.
4. Likhtman, A. E.; McLeish, T. C. B. Macromolecules 2002, 35, 6332.
5. Rubinstein, M.; Colby, R. H. J Chem Phys 1988, 89, 5291.
6. Doi, M. J Polym Sci Polym Lett Ed 1981, 19, 265.
7. Milner, S. T.; McLeish, T. C. B. Phys Rev Lett 1998, 85, 725.
8. des Cloiseaux, J. Eur Phys Lett 1998, 5, 437.
9. Miros, A.; Vlassopoulos, D.; Likhtman, A. E.; Roovers, J. J Rheol 2003, 47, 163.
10. Marucci, G. J Non-Newtonian Fluid Mech 1996, 62, 279.
11. Graham, R. S.; Likhtman, A. E.; McLeish, T. C. B.; Millner, S. T. J Rheol 2003, 47, 1171.
12. Likhtman, A. E.; Graham, R. S. J Non-Newtonian Fluid Mech 2003, 114, 1.
13. Larson, R. G.; Sridhar, T.; Leal, L. G.; McKinley, G. H.; Likhtman, A. E.; McLeish, T. C. B. J Rheol 2003, 47, 809.
14. Fox, T. G.; Gratch, S.; Loshaek, S. In: Viscosity Relationships for Polymers in Bulk and Concentrated Solution; Eirich, F. R., Ed.; Rheology: Theory and Applications, Vol. 1; Academic Press: New York, 1956.
15. Fetters, L. J.; Lohse, D. J.; Richter, D.; Witten, T. A.; Zirkel, A. Macromolecules 1994, 27, 4639.
16. Locati, G.; Pegoraro, M.; Nichetti, D. Polym Eng Sci 1999, 39, 741.
17. Graessley, W. W. In: Viscoelasticity and Flow in Polymer Melts and Concentrated Solutions; Mark, J. E.; Eisenberg, A.; Graessley, W. W.; Mandel Kern, L.; Samulski, E. T.; Koenig, J. L.; Wignall, G. D., Eds.; Physical Properties of Polymers, 2nd ed.; ACS Professional Reference Book: Washington DC, 1993.
18. Raju, V. R.; Rachapudy, H.; Graessley, W. W. J Polym Sci 1979, 17, 1223.
19. Carella, J. M.; Graessley, W. W.; Fetters, L. J. Macromolecules 1984, 17, 2775.
20. Fetters, L. J.; Lohse, D. J.; Milner, S. T.; Graessley, W. W. Macromolecules 1999, 32, 6847.
21. Pearson, D. S.; Fetters, L. J.; Graessley, W. W.; Ver Strate, G.; von Meerwall, E. Macromolecules 1994, 27, 711.
22. Schieber, J. D., Department of Chemical Engineering, Illinois Institute of Technology Chicago, Illinois, Personal communication, 2003.
23. Majeste, J. C.; Montfort, J. P.; Allal, A.; Marin, G. Rheol Acta 1998, 37, 486.
24. Schausberger, A.; Schindlauer, G.; Janeschitz-Kriegl, H. Rheol Acta 1985, 24, 220.
25. Graessley, W. W.; Roovers, J. Macromolecules 1979, 12, 959.